ICEE 2026: 32nd International Council on Electrical Engineering Conference, July 5-9, 2026, KCCI, Seoul, Korea

A Stator Permanent Magnet based Dual-rotor Synchronous Machine with Integrated Winding

Zhouyang Zhang*, Mingyuan Jiang†*, Zixu Dong*, Zhang Zhang*, Shuangxia Niu*, K. T. Chau* and C. C. Chan*

Abstract – Permanent magnet (PM) motors are widely adopted in high-performance drive systems due to their high-power density and dynamic response. However, conventional single-rotor topologies fall short in applications requiring multi-degree-of-freedom motion control. Dual-rotor configurations with a shared stator address this issue by enabling independent rotor control and expanding the torque-speed range, yet they suffer from mechanical reliability issues caused by centrifugal forces on rotor-PMs. Flux-switching (FS) motors offer a robust alternative with inherently low torque ripple by positioning excitation sources on the stator. This paper proposes a dual-rotor PM synchronous motor (PMSM) with spoke-type stator-PM placed in the middle of the stator slots. The proposed configuration eliminates the risk of PM detachment and enhances mechanical robustness, while an integrated winding simplifies the structure and increases control flexibility. Simulation results validate its electromagnetic decoupling and overall performance.

Keywords: Dual-rotor, FS, Stator-PM, PMSM

1. Introduction

Amid the global energy transition, the automotive and aerospace sectors are demanding increasingly stringent performance from electric drive systems. PM machines have become the better choice for high-performance applications due to their high-power density, efficiency, and dynamic response, playing an important role in emerging fields such as electric vehicles [1][2], hybrid electric vehicles [3][4], wind power generation [5][6], and wave energy conversion [7][8]. Permanent magnet (PM) brushless machines, such as the PM synchronous machines (PMSMs) [9][10], PM vernier machines [11][12], magnetic-geared PM machines [13][14] and stator-PM machines [15][16], exhibit definite advantages over the conventional DC machines [17][18], induction machines [19][20] and reluctance machines [21][22] in terms of efficiency, reliability and torque density.

Despite these developments, conventional single-rotor designs are increasingly inadequate in meeting the stringent efficiency and compactness prerequisites of advanced automotive and aerospace applications within the context of global energy transition [23]. Moreover, the rise of low-altitude aviation has intensified the need for motor topologies capable of multi-degree-of-freedom coordinated motion, particularly for electric vertical take-off and landing vehicles (eVTOLs) and robotic systems [24].

The dual-rotor PM machine features a coaxial structure in which two independent rotors share a common stator, enabling decoupled rotational control and enhanced torque output through coordinated magnetic circuit design [25][26]. However, practical deployment faces key technical challenges, including centrifugal forces from high-speed rotation that threaten the retention and reliability of rotor-PMs. Meanwhile, complex electromagnetic interactions between the dual rotors and stator windings create concentrated losses that hurt heat dissipation and system stability, while also generating force ripples that cause vibration and noise. [27][28]. Additionally, by using two independent windings with different pole numbers, each winding occupies an independent slot area. This will directly reduce the slot filling factor and increase copper loss. Addressing these challenges through advanced structural optimization is essential to fully leverage dual-rotor topologies for future high-performance applications.

The adoption of integrated winding configurations offers a compelling solution to the mentioned challenges. By enabling increased electrical loading under equivalent copper loss conditions, this topology achieves enhanced torque production capability relative to conventional dual-winding arrangements. Through current superposition and vector synthesis, the integrated winding generates two

† Corresponding Author: Mingyuan Jiang(m.y.jiang@polyu.edu.hk)
* Dept. of Electrical and Electronic Engineering, The Hong Kong Polytechnic University, Hong Kong, China
(zhouyang.zhang@connect.polyu.hk)

independent magnetomotive forces with distinct pole-pair numbers, enabling decoupled multi-rotor control while improving slot fill factor and thermal management, with advanced control strategies such as model predictive control ensuring precise current regulation and robust dynamic response. [29][30]. This inherent characteristic facilitates decoupled multi-rotor control within a shared stator structure, while simultaneously improving slot fill factor and thermal management performance [31].

The flux-switching permanent magnet (FSPM) machine operates on air-gap permeance modulation, featuring stator-PMs and windings with a salient-pole rotor [32][33]. This topology inherently eliminates high-speed PM detachment, ensuring superior mechanical robustness over conventional rotor-PM designs [34][35]. Recent studies confirm that optimizing rotor salient-pole geometry as a magnetic modulator significantly enhances torque density while suppressing parasitic effects, positioning FSPM as a strong candidate for high-performance traction applications [36]. Furthermore, the integrated winding arrangement facilitates decoupled multi-rotor operation without compromising mechanical integrity or torque output, culminating in an advanced stator-PM architecture ideally suited for multi-degree-of-freedom motion control.

This paper presents a novel stator PM dual-rotor motor topology with a distinctive configuration arrangement. The proposed design incorporates integrated windings alongside PMs positioned tangentially in the middle of the stator slots to enhance flux distribution. Such a configuration promotes efficient magnetic flux utilization, while the optimized flux path geometry aids in mitigating eddy current and magnetic reluctance losses, making the topology more well-suited for high-speed and high-overload applications [37]. The proposed topology offers notable advantages in terms of reliability, disturbance resilience, and cost efficiency for advanced motor systems operating under demanding conditions. Additionally, the use of integrated windings enables fully independent rotation of the two rotors, thereby providing enhanced control flexibility and more effective power allocation between the two mechanical ports.

2. Proposed Motor Structure

The topology of the proposed machine is shown in Fig. 1. The stator assembly accommodates the integrated winding, PMs tangentially placed in the middle of the stator slots, and two concentric rotors. This motor has 18 stator slots. The two rotors feature 14 and 17 salient teeth respectively, and the number of pole pairs generated by the integrated winding is equivalent to that of the equivalent separated windings of 5 pairs and 8 pairs respectively. The governing relationship between the stator and rotor pole combinations is defined by the followings:

$$P_s = \frac{Z}{2} \tag{1}$$

$$P_a = |P_s \pm N_k| \tag{2}$$

where P_s and P_a denotes the pole pair number of stator PMs and armature windings, Z corresponds to the number of stator slots, and N_k indicates the number of rotor teeth. The proposed structure is provided in Fig. 2, with the basic parameters of the proposed topology summarized in Table I.

Table 1. The basic parameters of proposed topology.

Item	Unit	Value
Number of stator slot	-	18
Teeth number of rotor 1	-	14
Teeth number of rotor 2	-	17
Pole pair number of Integrated Winding	-	5/8
Stack length of the motor	mm	50
Volume of PM	dm³	28.8
Outer diameter of the motor	mm	100
Speed of rotor 1	rpm	5000
Speed of rotor 2	rpm	-5000

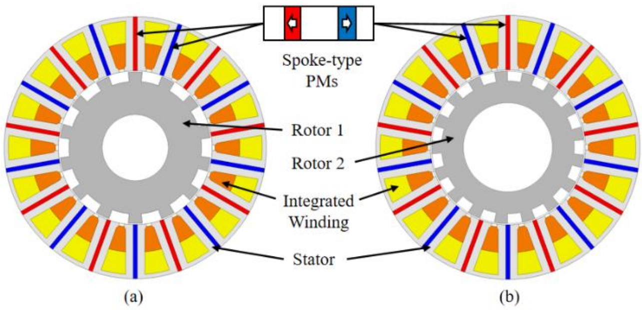

Fig. 1. The topology of the propose motor. (a) Front view, $N_{k1} = 14$. (b) Rear view, $N_{k2} = 17$.

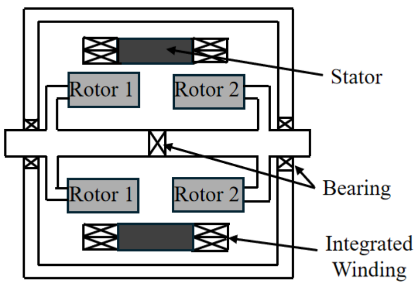

Fig. 2. The diagram of the proposed dual-rotor structure.

3. Operation Principle

3.1 Flux-Switching Modulation Principle

Based on the unified theory of air-gap field modulation in electrical machines, the air-gap flux density B is determined by the product of the MMF source and the permeance distribution [38]. This fundamental relationship is expressed as:

$$B=\Lambda\cdot F \tag{3}$$

where F denotes the MMF generated by excitation sources such as PMs or armature windings, while Λ represents the air-gap permeance function, which captures the periodic variation of the magnetic circuit arising from rotor saliency or modulating elements. The product of these two quantities characterizes the modulation process: the spatially distributed MMF, stationary or rotating, is modulated by the position-dependent permeance, generating a spectrum of harmonic components within the air-gap field. The MMF produced by stator-PMs remains stationary in space, whereas the rotor saliency imposes a periodic modulation on the air-gap permeance [39]. The MMF term describes the spatial distribution of the field source, while the permeance function represents the modulation effect of the magnetic circuit. Their interaction yields the air-gap flux density harmonics that underpin electromechanical energy conversion.

The final resulting air-gap flux density is obtained by multiplying the PM-excited MMF with the permeance function. For a rotor comprising N_k salient teeth, the permeance function exhibits a fundamental spatial harmonic whose period corresponds to N_k cycles per mechanical revolution [40]. The modulation of the PM MMF, characterized by a certain pole-pair number P_r, by this permeance harmonic gives rise to flux density components whose pole-pair numbers are determined by:

$$P_{m,n}=|mP_r \pm nN_k| \tag{4}$$

where m and n denote positive integers corresponding to the harmonic indices of the MMF and permeance functions, respectively. In practice, the armature winding is intentionally designed to couple with a particular harmonic field, generally the component possessing the highest magnitude, which constitutes the working harmonic responsible for torque production. In the proposed configuration, the PMs are arranged in a spoke-type configuration in the middle of the stator slots, thereby establishing a magnetic field characterized by a pole-pair number of $P_s = Z/2 = 9$ pole pairs. The two rotors feature distinct tooth counts, specifically $N_{k1} = 14$ and $N_{k2} = 17$, which give rise to different working harmonic components for each rotor. As determined by equation (2), the pole-pair numbers of the armature windings are selected as $P_{a1} = 5$ and $P_{a2} = 8$, corresponding to the fundamental modulation products derived from the interaction between the stator field and the respective rotor teeth:

$$P_{a1}|_{m=1,\,n=-1}=|P_s\text{-}N_{k1}|=|9\text{-}14|=5 \tag{5}$$

$$P_{a2}|_{m=1,\,n=-1}=|P_s\text{-}N_{k2}|=|9\text{-}17|=8 \tag{6}$$

Hence, each rotor independently modulates the PM field, producing rotating harmonics that interact with its dedicated winding. The harmonic component whose pole-pair number aligns with that of the armature winding becomes the effective working field, facilitating electromechanical energy conversion through air-gap modulation. This harmonic-based principle fundamentally differentiates FS machines from conventional synchronous machines, where torque arises solely from the fundamental field. Moreover, some FS machines exploit tailored higher-order harmonics, such as the third harmonic, to significantly improve torque density, confirming the practical value of harmonic utilization [41].

3.2 Integrated Winding Configuration

The principle of vector addition governs the production of dual MMFs in an integrated winding. Taking two equivalent separated windings with pole-pair numbers P_{a1} and P_{a2}, their phase-X currents are represented by $I_{x,1}$ and $I_{x,2}$. Under parallel connection with the same polarity, the resultant currents in the integrated winding are formed by the sum of these two components; whereas series connection with reversed polarity results in their subtraction. The instantaneous branch currents are expressed as:

$$\begin{aligned} i_{u,1} &= I_{u,I} + I_{u,II} \\ &= I_{m,I}\cos(\omega_I t + \phi_I + \theta_u) + I_{m,II}\cos(\omega_{II} t + \phi_{II} + \theta_u) \end{aligned} \tag{7}$$

$$\begin{aligned} i_{u,2} &= I_{u,I} - I_{u,II} \\ &= I_{m,I}\cos(\omega_{\mathrm{I}} t + \phi_{\mathrm{I}} + \theta_u) - I_{m,II}\cos(\omega_{\mathrm{II}} t + \phi_{\mathrm{II}} + \theta_u) \end{aligned} \tag{8}$$

where u denotes a specific phase within the three-phase winding system. θ_u represents its corresponding spatial phase angle, where $\theta_U = 0$, $\theta_V = 120°$, and $\theta_W = -120°$. ω_I and ω_{II} are the angular frequencies of the currents in the two equivalent separated windings, ϕ_I and ϕ_{II} are their respective initial phase angles of the currents in the two equivalent separated windings. The terms $I_{u,I}$ and $I_{u,II}$ represent the currents in phase U of the two equivalent separated windings with pole-pair number P_{a1} and P_{a2}, respectively.

Through addition or subtraction of the aforementioned branch currents, the currents corresponding to the equivalent separate windings can be expressed:

$$I_{u,I}=\frac{i_{u,1}+i_{u,2}}{2} \tag{9}$$

$$I_{u,II}=\frac{i_{u,1}\text{-}i_{u,2}}{2} \tag{10}$$

This superposition principle underpins the independent control of two distinct magnetic fields within a single winding structure. The winding configuration of the proposed integrated design is illustrated in Fig. 3, where a coil pitch of one slot is employed and the interphase connections are schematically depicted.

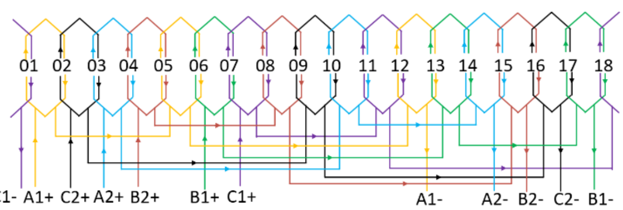

Fig. 3. The winding arrangement of the proposed combination.

Although physically integrated, the two conceptual windings inherently share a common magnetic circuit, resulting in unavoidable electromagnetic coupling. This interaction is quantified by the mutual flux linkage, which occurs when the flux density generated by one winding links the turns of the other. The mutual flux linkage in winding II due to excitation of winding I is derived from the integral of the product of the air-gap flux density distribution $B_I(\theta)$ and the winding function $M_{II}(\theta)$:

$$\Psi_{II,I}=l_{stk}R_{gap}\int_0^{2\pi} B_I(\theta)M_{II}(\theta)\ d\theta \qquad (11)$$

where l_{stk} denotes the stack length and R_{gap} represents the air-gap radius. Fourier expansion reveals that only spatial harmonics common to both distributions contribute to mutual flux. Decoupling between the windings is attained when the sets of nonzero harmonic orders of M_{II} and B_I are mutually exclusive, meaning the harmonics present in the flux density of one winding do not coincide with those of the winding function of the other. This condition ensures that the mutual inductance becomes zero, thereby enabling fully independent control of each rotor without undesirable cross-coupling. Fig. 4 presents the decoupling verification results for the 5-8 winding pole-pair combination, where $A,1$ and $A,2$ represent the back EMF of the phase-A for the 5-pole pair and 8-pole pair windings, respectively. The presence of a smooth sinusoidal waveform alongside a nearly zero curve in Fig. 4 confirms the decoupled operation of this configuration.

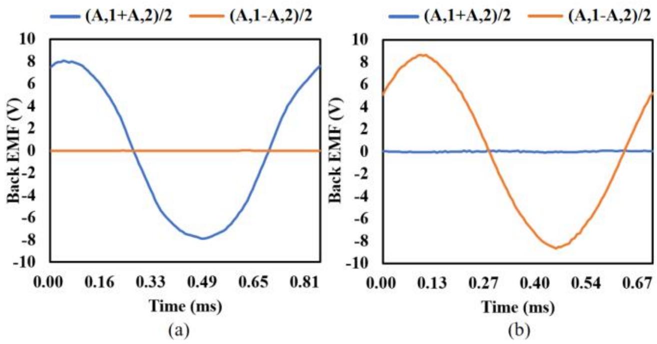

Fig. 4. The decoupling verification for 5-8 winding pole pair combination. (a) $n_{r1}=5000rpm,\ n_{r2}=0$. (b) $n_{r1}=0,\ n_{r2}=-5000rpm$.

4. Performances

To evaluate the performances of the proposed topology, finite element method (FEM) simulations were performed under both no-load and on-load conditions.

4.1 Optimization

A systematic multi-objective optimization was undertaken, focusing on two critical performance indices: torque density (K_T) and torque ripple (T_r) with the goal of achieving an optimal trade-off between them. The resultant performance characteristics are presented in Table II, and the optimized parameters are summarized in Table III. As a result of the optimization, the torque density of the 5-pole rotor (K_{T1}) and 8-pole rotor (K_{T2}) achieve 5.71 and 5.34 Nm/L, respectively.

Table 2. The optimized structural performance.

Items	Unit	Value
T_{avg1}	Nm	2.24
T_{avg2}	Nm	2.10
T_{r1}	%	7.79
T_{r2}	%	5.21
K_{T1}	Nm/L	5.71
K_{T2}	Nm/L	5.34

Table 3. The optimized structural parameters.

Items	Unit	Value
Outer diameter of the motor	mm	100
Stack length of the motor	mm	50
Volume of PM, V_{PM}	dm³	28.8
Width of PMs, b_{pm}	mm	1.55
Yoke of stator, hy_s	mm	1.59
Width between stator slots, bt_o	mm	7.35
Height of stator slots, hs_0	mm	17.05
Yoke of rotor 1, hy_{r1}	mm	13.27
Pole arc ratio of rotor 1, $alfri_1$	-	1.18
Height of rotor1 teeth, ht_{r1}	mm	3.59
Yoke of rotor 2, hy_{r2}	mm	9.00
Pole arc ratio of rotor 2, $alfri_2$	-	1.07
Height of rotor2 teeth, ht_{r2}	mm	3.74

4.2 No-load analysis

The left portion of each model of Fig. 5 illustrates the flux line distribution under no-load condition. A relatively uniform distribution of magnetic flux lines is clearly observed throughout the core during no-load operation.

Fig. 6 illustrates the back EMF waveforms of the integrated winding. It can be observed that the back EMF waveforms of the integrated windings exhibit non-sinusoidal characteristics. By applying equations (9) and (10), the back EMF waveforms corresponding to the two equivalent separated windings are derived, exhibiting regular sinusoidal characteristics. Fig. 7 shows the equivalent separated winding waveforms, acquired at 5000 rpm with the two rotors rotating in opposite directions. The first winding set, characterized by 5 pole pairs, displays an amplitude of 8.0 V, while the second set with 8 pole pairs, shows an amplitude of 8.6 V. Subsequent validation confirms that the performance of the integrated winding is essentially consistent with that of its equivalent separated counterparts.

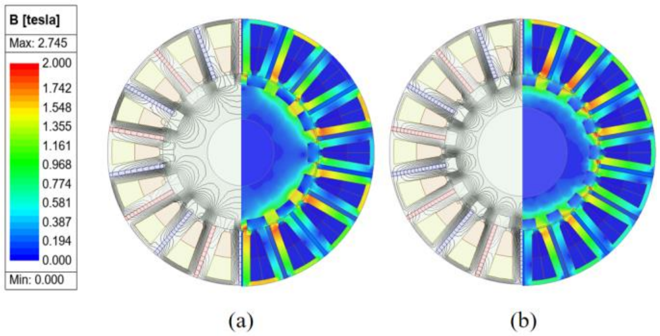

Fig. 5. The no-load flux line distribution and on-load flux density map of the proposed rotors. (a) Front view. (b) Rear view.

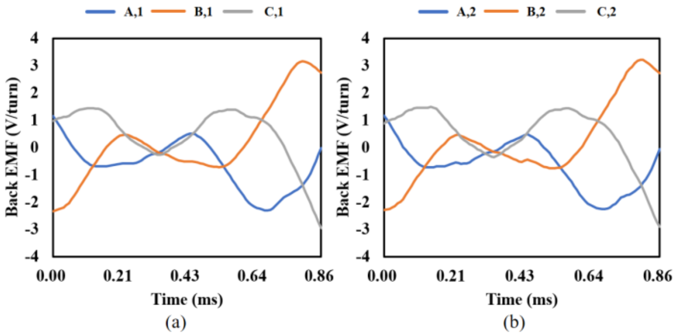

Fig. 6. The integrated winding waveforms of back EMF of the proposed structure. (a) $P_{a1} = 5$. (b) $P_{a2} = 8$.

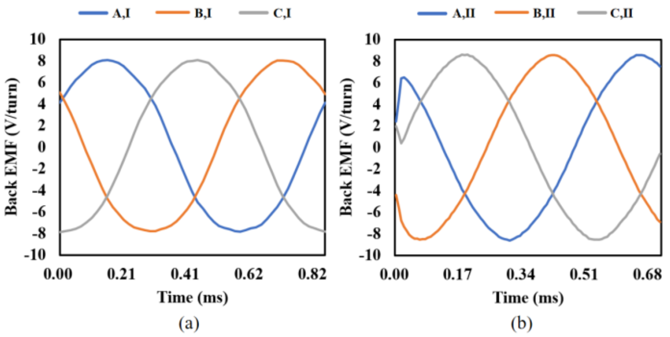

Fig. 7. The equivalent separated winding waveforms of back EMF of the proposed structure. (a) $P_{a1} = 5$. (b) $P_{a2} = 8$.

4.3 Load analysis

The on-load flux density distribution is presented in the right portion of each model in Fig. 5, revealing generally favorable magnetic field intensity levels across most regions. Fig. 8 depicts the torque waveforms for both the 5-pole and 8-pole rotor configurations, demonstrating relatively stable torque output in both cases. Among them, the average torque of the 5-pole rotor (T_{avg1}) and 8-pole rotor (T_{avg2}) are 2.24 and 2.10 Nm, respectively, with corresponding torque ripples (T_{r1}, T_{r2}) are 7.79% and 5.21%, respectively. Both of the T_r fall below the conventional 10% benchmark, indicating satisfactory operational smoothness. The T_{avg} of these two rotors is relatively excellent, and the consistently low T_r also confirms the outstanding stability characteristics of the proposed design.

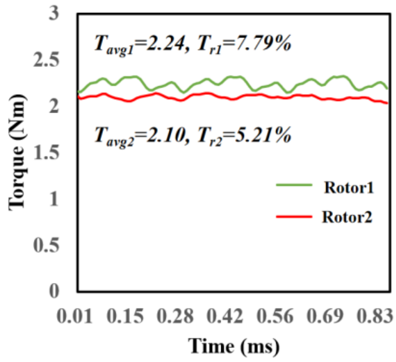

Fig. 8. The torque waveforms of the proposed rotors.

5. Conclusion

This paper presents a novel dual-rotor PM motor topology with stator-PMs arranged in a distinctive spatial configuration. The proposed design integrates integrated winding with tangentially oriented PMs positioned in the middle of the stator slots, thereby inherently eliminating the risk of PM detachment associated with conventional rotor-PM machines under high-speed operation. By facilitating independent rotational control of both rotors within a compact stator assembly, the topology naturally supports fault-tolerant operation and promotes system integration, rendering it particularly well-suited for safety-critical applications where spatial limitations and operational redundancy are essential considerations. The FEM performance evaluation indicates that the proposed design has relatively excellent torque density. The torque density of the two rotors are 5.71 Nm/L and 5.34 Nm/L respectively. At the same time, the low torque ripples, which are 7.79% and 5.21% respectively, also prove its remarkable stability. Consequently, the proposed FS single-stator dual-rotor PM motor topology demonstrates both commendable electromagnetic characteristics and superior stability, positioning it as a promising candidate for advanced motion control applications.

Acknowledgements

This work was supported by The Hong Kong Polytechnic University under Projects P0056361 and P0052647.

References

[1] K. T. Chau, “Pure electric vehicles,” Alternative Fuels and Advanced Vehicle Technologies for Improved Environmental Performance, Woodhead Publishing, pp. 655-684, Mar. 2014.

[2] W. X. Shen, K. T. Chau, C. C. Chan, and E. W. C. Lo, “Neural network based residual capacity indicator for nickel-metal hydride batteries in electric vehicles,”

IEEE Trans. Veh. Technol., vol. 54, no. 5, pp. 1705-1712, Sep. 2005.

[3] K. T. Chau and C. C. Chan, “Emerging energy-efficient technologies for hybrid electric vehicles,” Proceedings of the IEEE, vol. 95, no. 4, pp. 821-835, Apr 2007.

[4] X. Zhang, K. T. Chau and C. C. Chan, “Overview of thermoelectric generation for hybrid vehicles,” J. Asian Electr. Veh., vol. 6, no. 2, pp. 1119-1124, Dec. 2008.

[5] H. Chen, Y. Zuo, K. T. Chau, W. Zhao, and C. H. T. Lee, “Modern electric machines and drives for wind power generation: A review of opportunities and challenges,” IET Renew. Power Gener., vol. 15, no. 9, pp. 1864-1887, Jul. 2021.

[6] Z. Dong, M. Jiang, S. Niu and K. T. Chau, "Overview of Permanent Magnet Wind Power Generators," in *IEEE Transactions on Magnetics*, vol. 61, no. 9, pp. 1-11, Sep. 2025.

[7] Y. Du, K. T. Chau, M. Cheng, Y. Fan, W. Zhao, and F. Li, “A linear stator permanent magnet vernier HTS machine for wave energy conversion,” IEEE Trans. Appl. Supercond., vol. 22, no. 3, p. 5202505, pp. 1-5, Jun. 2012.

[8] T. W. Ching, K. T. Chau, and W. Li, “Power factor improvement of a linear vernier permanent-magnet machine using auxiliary DC field excitation,” IEEE Trans. Magn., vol. 52, no. 7, p. 8204804, pp. 1-4, Jul. 2016.

[9] L. Jian, K. T. Chau, Y. Gong, C. Yu, and W. Li, “Analytical calculation of magnetic field in surface-inset permanent magnet motors,” IEEE Trans. Magn., vol. 45, no. 10, pp. 4688-4691, Oct. 2009.

[10] Y. Wang, M. Cheng, M. Chen, Y. Du, and K. T. Chau, “Design of high-torque-density double-stator permanent magnet brushless motors,” IET Electr. Power Appl., vol. 5, no. 3, pp. 317-323, Mar. 2011.

[11] X. Li, K. T. Chau, and M. Cheng, “Comparative analysis and experimental verification of an effective permanent-magnet vernier machine,” IEEE Trans. Magn., vol. 51, no. 7, p. 8203009, pp. 1-9, Jul. 2015.

[12] J. Li, K. T. Chau, and W. Li, “Harmonic analysis and comparison of permanent magnet vernier and magnetic-geared machines,” IEEE Trans. Magn., vol. 47, no. 10, pp. 3649-3652, Oct. 2011.

[13] L. Jian, K. T. Chau and J. Z. Jiang, "An Integrated Magnetic-Geared Permanent-Magnet In-Wheel Motor Drive for Electric Vehicles, " IEEE Vehicle Power and Propulsion Conference, pp. 1-6, Sep. 2008.

[14] C. Liu, K.T. Chau and Z. Zhang, “Novel design of double-stator single-rotor magnetic-geared machines” IEEE Trans. Magn., vol. 48, no. 11, pp. 4180-4183, Nov. 2012.

[15] S. Niu, S. Wang and X. Zhao, "Overview of Stator Slot-Opening Permanent Magnet Machines," in *IEEE Transactions on Transportation Electrification*, vol. 9, no. 1, pp. 782-804, March 2023.

[16] D. Li, Y. Gao, R. Qu, J. Li, Y. Huo and H. Ding, "Design and Analysis of a Flux Reversal Machine With Evenly Distributed Permanent Magnets," in *IEEE Transactions on Industry Applications*, vol. 54, no. 1, pp. 172-183, Jan.-Feb. 2018.

[17] J. H. Chen, K. T. Chau, S. M. Siu, and C. C. Chan, “Experimental stabilization of chaos in a voltage-mode DC drive system,” IEEE Trans. Circuits Syst. I: Fundam. Theory Appl., vol. 47, no. 7, pp. 1093-1095, Jul. 2000.

[18] Z. Wang and K. T. Chau, “Anti-control of chaos of a permanent magnet DC motor system for vibratory compactors,” Chaos Solitons Fractals, vol. 36, no. 3, May 2008, pp. 694-708.

[19] C. C. Chan, L. Yan, P. Chen, Z. Wang and K. T. Chau, “Analysis of electromagnetic and thermal fields for induction motors during starting,” IEEE Trans. Energy Convers., vol. 9, no. 1, pp. 53-60, Mar. 1994.

[20] S. Z. Jiang, K. T. Chau, and C. C. Chan, “Spectral analysis of a new six-phase pole-changing induction motor drive for electric vehicles,” IEEE Trans. Ind. Electron., vol. 50, no. 1, pp. 123-131, Feb. 2003.

[21] Y. Gao and K. T. Chau, “Hopf bifurcation and chaos in synchronous reluctance motor drives,” IEEE Trans. Energy Convers., vol. 19, no. 2, pp. 296-302, Jun. 2004.

[22] J. H. Chen, K. T. Chau, C. C. Chan, and Q. Jiang, “Subharmonics and chaos in switched reluctance motor drives,” IEEE Trans. Energy Convers., vol. 17, no. 1, pp. 73-78, Mar. 2002.

[23] Z. Dong, M. Jiang and Z. Huang, "Guideline of Integrated Winding for Dual Mechanical-Port Machines," *2025 IEEE 20th Conference on Industrial Electronics and Applications (ICIEA)*, Yantai, China, 2025, pp. 1-6.

[24] L. Dai, S. Niu, Z. Lyu, X. Huang and K. T. Chau, "Challenges and Opportunities in Electric Propulsion Systems for Low-Altitude eVTOL Aircraft," in *IEEE Transactions on Power Electronics*.

[25] M. Jiang and S. Niu, "A Novel Consequent-Pole Contra-Rotating Machine With Zero-Sequence Current Excitation," in *IEEE Transactions on Magnetics*, vol. 59, no. 11, pp. 1-5, Nov. 2023, Art no. 8101405.

[26] M. Jiang and S. Niu, "Overview of Dual Mechanical Port Machines in Transportation Electrification," in *IEEE Transactions on Transportation Electrification*, vol. 10, no. 3, pp. 4959-4977, Sept. 2024.

[27] Z. Huang, M. Jiang, S. Niu, Z. Lyu, W. Wu and L. Xiao, "A Novel Hybrid-Flux Dual-Mechanical-Port Dual-Electrical-Port Machine for Hybrid Electric Vehicles," in *IEEE Transactions on Industrial Electronics*, vol. 73, no. 1, pp. 149-159, Jan. 2026.

[28] C. Huang, L. Xiong, Y. Gong, M. Jiang and S. Niu, "Tangential Electromagnetic Force Array on the Vibration and Noise of Electric Axle for New Energy Vehicle," in *IEEE Access*, vol. 11, pp. 100001-100009, 2023.

[29] X. Ren, D. Li, R. Qu, X. Han and Z. Liang, "A Brushless Dual-Electrical-Port Dual-Mechanical-Port Machine With Integrated Winding Configuration," in *IEEE Transactions on Industrial Electronics*, vol. 68, no. 4, pp. 3022-3032, April 2021.

[30] S. Niu, Y. Luo, W. Fu and X. Zhang, "Robust Model Predictive Control for a Three-Phase PMSM Motor With Improved Control Precision," in *IEEE*

Transactions on Industrial Electronics, vol. 68, no. 1, pp. 838-849, Jan. 2021.

[31] X. Fan, B. Zhang, R. Qu, D. Li, J. Li and Y. Huo, "Comparative Thermal Analysis of IPMSMs With Integral-Slot Distributed-Winding (ISDW) and Fractional-Slot Concentrated-Winding (FSCW) for Electric Vehicle Application," in *IEEE Transactions on Industry Applications*, vol. 55, no. 4, pp. 3577-3588, July-Aug. 2019.

[32] Z. Q. Zhu and J. T. Chen, "Advanced Flux-Switching Permanent Magnet Brushless Machines," in *IEEE Transactions on Magnetics*, vol. 46, no. 6, pp. 1447-1453, June 2010.

[33] W. Zhao, M. Cheng, K. T. Chau, W. Hua, H. Jia, J. Ji, and W. Li, "Stator-Flux-Oriented Fault-Tolerant Control of Flux-Switching Permanent-Magnet Motors," in *IEEE Transactions on Magnetics*, vol. 47, no. 10, pp. 4191-4194, Oct. 2011.

[34] C. Liu, K. T. Chau, and W. Li, "Comparison of Fault-Tolerant Operations for Permanent-Magnet Hybrid Brushless Motor Drive," in *IEEE Transactions on Magnetics*, vol. 45, no. 6, pp. 1378-1381, Jun. 2010.

[35] S. Niu, X. Zhao, X. Zhang and T. Sheng, "A Novel Axial-Flux-Complementary Doubly Salient Machine With Boosted PM Utilization for Cost-Effective Direct-Drive Applications," in *IEEE Access*, vol. 7, pp. 145970-145977, 2019.

[36] K. T. Chau, Y. B. Li, J. Z. Jiang, and C. Liu, "Design and Analysis of a Stator-Doubly-Fed Doubly-Salient Permanent-Magnet Machine for Automotive Engines," in *IEEE Transactions on Magnetics*, vol. 42, no. 10, pp. 3470-3472, Oct. 2006.

[37] M. Cheng, F. Yu, K. T. Chau, and W. Hua, "Dynamic Performance Evaluation of a Nine-Phase Flux-Switching Permanent Magnet Motor Drive With Model Predictive Control," in *IEEE Transactions on Industrial Electronics*, vol. 63, no. 7, pp. 4539-4549, Jul. 2016.

[38] M. Cheng; P. Han; Y. Du; H. Wen, "Performance Evaluation of Electrical Machines Based on General Airgap Field Modulation Theory," in *General Airgap Field Modulation Theory for Electrical Machines: Principles and Practice* , IEEE, 2023, pp.227-292.

[39] Z. Z. Wu and Z. Q. Zhu, "Analysis of Air-Gap Field Modulation and Magnetic Gearing Effects in Switched Flux Permanent Magnet Machines," in *IEEE Transactions on Magnetics*, vol. 51, no. 5, pp. 1-12, May 2015, Art no. 8105012.

[40] Y. Du, F. Xiao, W. Hua, X. Zhu, M. Cheng, L. Quan, and K. T. Chau, "Comparison of Flux-Switching PM Motors With Different Winding Configurations Using Magnetic Gearing Principle," in *IEEE Transactions on Magnetics*, vol. 52, no. 5, pp. 1-8, May 2016, Art no. 8201908.

[41] M. Jiang and S. Niu, "A High-Order Harmonic Compound Rotor Based Brushless Dual-Electrical-Port Dual-Mechanical-Port Machine," in *IEEE Transactions on Industrial Electronics*, vol. 71, no. 6, pp. 5463-5473, June 2024.

Zhouyang Zhang
Zhouyang Zhang received the B.Eng. degree in Robotics Engineering from Wuhan University of Technology, Wuhan, China, in 2025. He is currently working toward the M.Phil. degree in electrical engineering with Department of Electrical and Electronic Engineering, The Hong Kong Polytechnic University, Hong Kong, China. His research interests include electric vehicles and machine design.

Mingyuan Jiang
Mingyuan Jiang received the B.Eng. degree in Electrical Engineering and Automation from Shanghai Maritime University, Shanghai, China, in 2020. He subsequently obtained his M.Sc. and Ph.D. degrees in Electrical Engineering from The Hong Kong Polytechnic University, Hong Kong, China, in 2021 and 2024, respectively.
He is currently a Research Assistant Professor in the Department of Electrical and Electronic Engineering and a member of the Research Centre for Electric Vehicles (RCEV) at The Hong Kong Polytechnic University. He is currently the Guest Editor and long-term reviewer for several well-known SCI journals. His primary research interests include the design, optimization, and control of electric machines, transportation electrification, robotics, and power generation systems.

Zixu Dong
Zixu Dong received the B.Eng. degree in electrical engineering and automation from Taiyuan University of Technology, Taiyuan, China in 2021. Subsequently, he obtained the M.Sc. degrees in electrical engineering from The Hong Kong Polytechnic University, Hong Kong, China, in 2025. He is currently working toward the Ph.D. degree in the Department of Electrical and Electronic Engineering, The Hong Kong Polytechnic University, Hong Kong, China. His research interests include design, optimization, and control of electric machines, electric vehicles, and power generation.

Zhang Zhang
Zhang Zhang received the B.Eng. degree in automation from the University of South China, Hengyang, China, in 2022, and the M.Eng. degree in control engineering from Shenzhen University, Shenzhen, China, in 2025. He is currently working toward the Ph.D.

degree in electrical engineering with Department of Electrical and Electronic Engineering, The Hong Kong Polytechnic University, Hong Kong, China. His research interests include servo motor drives, control theory, and intelligent systems.

Shuangxia Niu

Shuangxia Niu received the B.Sc. and M.Sc. degrees in electrical engineering from Tianjin University, Tianjin, China, in 2002 and 2005, respectively, and the Ph.D. degree in electrical engineering from the University of Hong Kong, Hong Kong, China, in 2009.
She is currently a Professor with the Department of Electrical and Electronic Engineering, The Hong Kong Polytechnic University, Hong Kong. She has authored or coauthored more than 100 papers in leading journals. er research interests include the electric vehicle technologies, renewable energy systems, machines and drives, power electronics technology, applied electromagnetic, numerical method, and optimization.

K.T. Chau

K.T. Chau received the B.Sc. (Eng.), M.Phil., and Ph.D. degrees in electrical and electronic engineering from The University of Hong Kong, Hong Kong, China, in 1988, 1991, and 1993, respectively.
He serves as a Chair Professor in electrical energy engineering with the Research Centre for Electric Vehicles and Department of Electrical and Electronic Engineering, The Hong Kong Polytechnic University, Hong Kong. His research interests include electric and hybrid vehicles, power electronics and drives, and renewable energies. He is the author of nine books and more than 350 journal papers.
He is a fellow of the Institution of Engineering and Technology (IET), U.K., and the Hong Kong Institution of Engineers. He is a Chartered Engineer. He was the recipient of the Changjiang Chair Professorship from the Ministry of Education, China, and the Environmental Excellence in Transportation Award for Education, Training, and Public Awareness from the Society of Automotive Engineers International.

C.C. Chan

C.C. Chan was born in 1937. He received the B.S. degree from China University of Mining and Technology, Xuzhou, China, in 1957, the M.S. degree from Tsinghua University, Beijing, China, in 1959, and the Ph.D. degree from the University of Hong Kong, Hong Kong, China, in 1982, all in electrical engineering. He is currently a Distinguished Chair Professor of electric vehicles and smart energy with the Department of Electrical and Electronic Engineering, Hong Kong Polytechnic University, Hong Kong. He has more than 50 years of teaching and research experience and proposes engineering philosophy, engineering, and education innovation, which laid the foundation of modern electric vehicles theory and electric vehicles electric drive theory. He has authored more than 300 papers and 11 monographs. Prof. Chan is a member of the Chinese Academy of Engineering and the Ukrainian Academy of Engineering Sciences, a fellow of the Royal Academy of Engineering U.K., and an Honorary Fellow of the Hungarian Academy of Engineering. He is a Senior IET Fellow and the Former President of the Hong Kong Institution of Engineers. He was a recipient of the Toastmasters Medal by the Institution of Electrical Engineers (IEE) in 2000, Father of Asian Electric Vehicles by Magazine Global View in 2003, Environmental Excellence in Transportation Award by the Society of Automotive Engineers (SAE) in 2007, Gold Medal of Hong Kong Institution of Engineers in 2010, World Federation of Engineering (WFEO) Medal for Engineering Excellence in 2013, Prince Philip Medal of U.K. Royal Academy of Engineering in 2014, and IEEE Transportation Technologies Award by IEEE in 2018.